DOI:
10.1002/adom.201600185

Document Version
Publisher's PDF, also known as Version of record

Silk-Based Biocompatible Random Lasing

Soraya Caixeiro, Michele Gaio, Benedetto Marelli, Fiorenzo G. Omenetto, and Riccardo Sapienza**

Lasers made from biological materials have the potential to produce new coherent light sources, flexible and compatible for living tissue integration. Biocompatible lasers are attracting attention for their potential to harness the amplifying power of stimulated emission for biosensing and cell tracking.[1] So far all-biological lasers have been devised using conventional lasing schemes, such as spherical microresonators,[2] microcavities,[3] and recently even implanted into live cells.[4,5] While high-Q cavities favor lasing, their precise geometry limits the applications for dynamic systems like living tissues. Instead, random lasing is emerging as a simple, robust, and easy to integrate, source of stimulated radiation, relying on disorder and multiple scattering to fold the optical paths inside the gain medium to trigger lasing.[6,7] Random lasing can be obtained in a variety of media, including organic materials such as cellulose,[8,9] and biological tissues.[10,11] Moreover, it is not influenced by the material's overall shape but instead it relies on its internal heterogeneity, therefore it can easily adapt to biological media with the ability to withstand stretching, wetness, and heat: its form is naturally biocompatible. A biocompatible device also requires the compatible chemistry of its constituents. Among many biopolymers, silk is emerging as a very versatile protein, biocompatible and biodegradable with outstanding mechanical properties,[12,13] that allows the fabrication of a variety of silk-based biomaterials.[14,15] Silk is especially suitable for photonic devices;[16,17] for instance, a conventional lasing architecture in silk has been reported, restricted to a glass substrate structured with a grating.[18,19]

Here, we demonstrate a biocompatible random laser made entirely of doped silk, functional in aqueous media, showing clear threshold behavior and spectral narrowing. Furthermore, this device is capable of probing changes in a chemical environment, namely, pH, due to the intrinsic nonlinear response and the large spectral purity.

The key ingredients to achieve random lasing are optical gain and a scattering medium. Bulk silk fibroin from *Bombyx Mori* silkworm is transparent; however, when nanostructured with pores with size comparable with the wavelength of light (≈100–1000 nm), the resulting inverted photonic glass efficiently scatters the incident light. We define the photonic glass to be direct if it is an assembly of silk sphere in air and inverted if it is composed of spherical voids in the silk matrix, i.e., the inverted structure. The fabrication protocol is shown in **Figure 1**a that describes the multiscale integration of the various components: dye molecules (sodium fluorescein or rhodamine 6G) are inserted in silk fibroin to be assembled and nanostructured into an inverse photonic glass and subsequently into a macroscopic random lasing device.

Photonic glasses are fabricated by destabilizing a colloidal solution to induce flocculation, which is usually achieved by adding a salt or an acid.[20] This step ensures a random packing of the spheres and avoids the formation of an opal structure.[21] Here instead, polystyrene spheres and silk are mixed together directly, as silk naturally destabilizes the colloidal solution. A photonic glass is grown directly by deposition, without the need for templating and infiltration which has been the fabrication route for 3D silk inverse opals.[16] The sample is dried in an oven and the silk is crystallized by exposing to water vapor. The polystyrene spheres are finally selectively removed by chemical etching in toluene, as shown in Figure 1b (see the Experimental Section).

Gain molecules, rhodamine and fluorescein laser dyes, are added to the solution of silk prior to casting. Fluorescein is biocompatible and extensively used for diagnostic purposes.[22] The dye molecules are encapsulated in the silk during the drying process, through hydrophobic interactions established with the protein. The result is a disordered silk matrix with connected spherical air voids (inset Figure 1c), which can be made free-standing (see the Experimental Section).

The silk scaffolding is expected to provide thermal dissipation and decrease intermolecular quenching, similar to that reported for DNA matrices.[23] This allows growing active and free-standing inverted photonic glasses made entirely of doped silk. In addition, the porous open architecture of the inverse photonic glass is ideal to entrain various biological and/or chemical dopants.

The silk inverted photonic glass is a strongly scattering medium, as characterized in **Figure 2**. The measured transport mean free path (l_t) is in the range $l_t \approx 3$–7 μm (blue line), with minor resonant modulations due to collective Mie scattering resonances, which can be engineered either by changing the diameter of the air voids or their refractive index. As a reference a direct photonic glass made of polystyrene spheres alone

S. Caixeiro, M. Gaio, Dr. R. Sapienza
Department of Physics
King's College London, Strand
London WC2R 2LS, UK
E-mail: Riccardo.Sapienza@kcl.ac.uk
Dr. B. Marelli, Prof. F. G. Omenetto
Department of Biomedical Engineering
Tufts University
4 Colby Street, Medford, MA 02155, USA
E-mail: Fiorenzo.Omenetto@tufts.edu
Prof. F. G. Omenetto
Department of Physics
Tufts University
4 Colby St., Medford, MA 02155, USA

DOI: 10.1002/adom.201600185

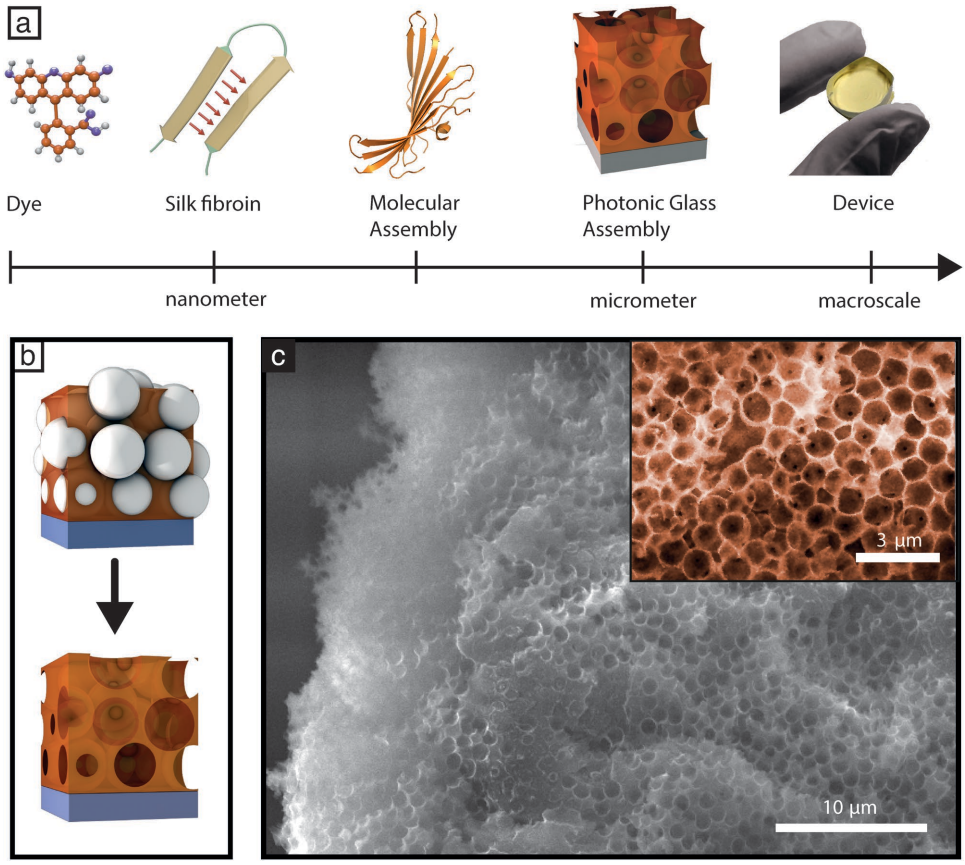

Figure 1. a) Material multiscale integration from the nanoscale to the macroscale. b) Sketch of the direct and inverse structure. c) A scanning electron microscopy image of the final structure and zoomed (pseudo-color) image in the inset, highlighting the air voids and the silk structure.

(red line in Figure 2) is also shown, presenting stronger scattering resonances and lower l_t values. These values have been obtained by recording the total light transmission through the undoped nanostructured silk of different thickness as a function of the light wavelength and by fitting the results with the optical Ohm's law (see the Experimental Section).[20] The thickness of the inverse silk photonic glass has been measured via scanning electron microscopy images, with an error smaller than 10% (statistical from repeated measurements). Instead, the thickness of the direct photonic glass has been estimated from the total volumes of sphere used, and has therefore a large systematic error as part of the sphere is lost deposited on the container; here the curve of mean free path for the direct photonic glass is underestimated and serves only as a comparison.

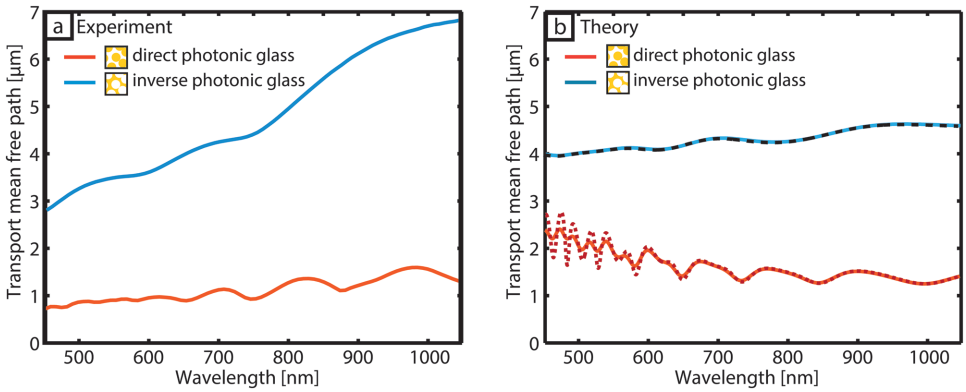

Figure 2. a) Measurements of the light transport mean free path for direct, polymer sphere in air (red) and inverse, air sphere in silk photonic glass (blue). b) Theoretical transport mean free path calculated for both direct and inverse geometries. Dashed lines: (red) polystyrene spheres with diameter $d = 1280$ nm and refractive index $n_{ps} = 1.6$ at filling fraction $f = 0.5$ and (blue) the inverse structure composed of air voids in silk, $n_{silk} = 1.6$. The solid lines are the same curves once the effect of the spheres size polydispersity (≈2%) is taken into account.

These experiments are compared to theoretical calculations in Figure 2b, via Mie theory and independent scattering approximation, including also the particle polydispersity (see the Experimental Section). As expected, while a polymer sphere in air is a good Mie resonator that efficiently traps the optical field owing to its high refractive index, an air void in a silk matrix induces smaller scattering resonances. Although a qualitative agreement between theory and experiment is evident, the shift in the resonances and intensity discrepancy are attributed to the limited validity of the independent scattering approximation for a closed-packed system such as the one investigated here.[6] The measured values of l_t in the silk inverted photonic glass give a dimensionless parameter $kl_t \approx 40$–60 (where k is the light wavevector), which indicates that silk inverted photonic glasses are strongly scattering biomaterials adequately described by diffusive models.

The dye-doped inverse silk photonic glass can act as a very efficient random lasing system, as proven in **Figure 3**. The crossover from fluorescent to lasing emission can be observed by recording the emission spectrum while increasing the exciting laser power. A sudden increase in the emitted light intensity is observed when the pump power reaches a critical value, i.e., the lasing threshold. The threshold occurs at 38 mJ cm^{-2} of pump energy for fluorescein and 7 mJ cm^{-2} for rhodamine, which compares favorably to similar systems in other material hosts, albeit not biocompatible.[24,25] The higher threshold of fluorescein is due to the lower absorption cross section at the pumping wavelength. After the threshold, stimulated emission becomes the dominant emission process and random lasing action occurs. In Figure 3a,c, the change of emission regime is marked by both a spectral narrowing (green full circles) and an increase of emission at the lasing wavelength (blue empty circles). The spectral linewidth is evaluated below threshold, at 27 mJ cm^{-2}, and above threshold, at 100 mJ cm^{-2}, for sodium fluorescein doped inverse photonic glass (Figure 3b) and for the rhodamine doped inverse photonic glass, below threshold at 4 mJ cm^{-2}, and well into the lasing regime at 160 mJ cm^{-2}. A small frequency shift of the emission upon increasing pumping energy is observed, from 559 to 552 nm for fluorescein, and from 578 to 589 nm for rhodamine, typical for random lasing, as the lasing frequency depends on the interplay of scattering and net gain.[25,26] The emission spectra are smooth curves as one would expect for diffusive or incoherent random lasing with non-resonant feedback.[6,7] The data can be modeled appropriately with a diffusive random lasing theory,[27] as we discuss in the Supporting Information.

When the random laser is operated in an aqueous environment such as a biological media, the scattering strength is

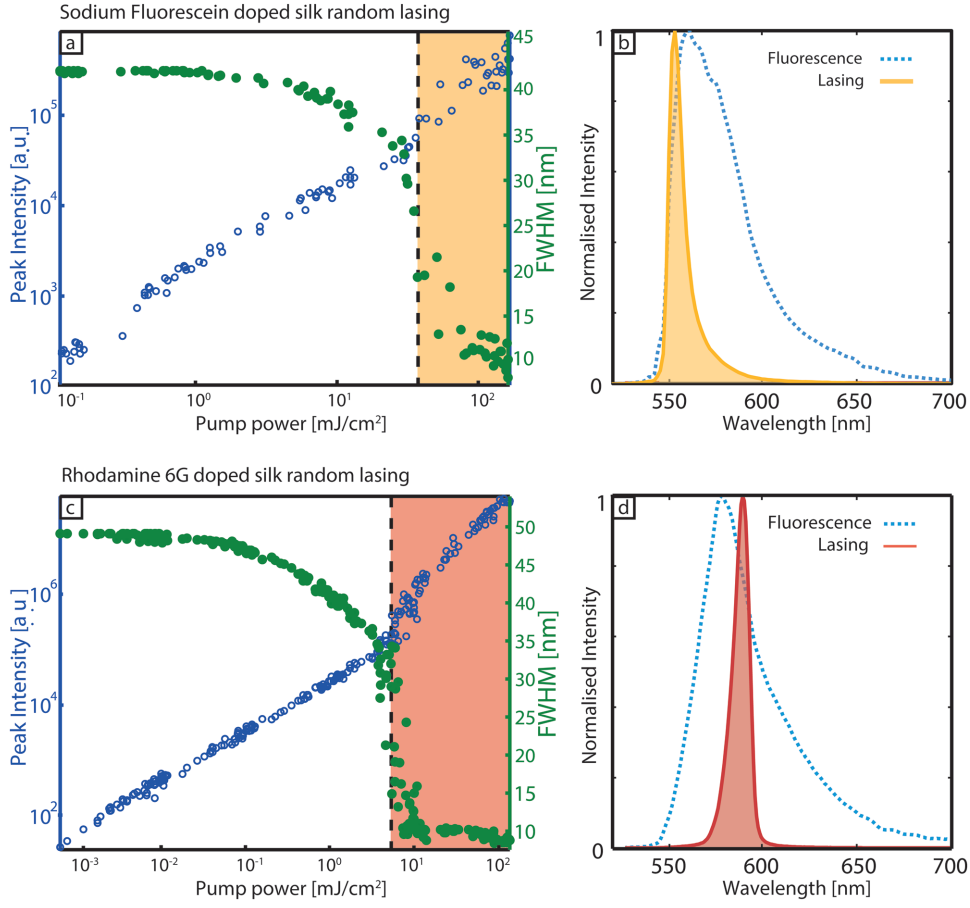

Figure 3. a,c) Typical lasing plot for silk doped with sodium fluorescein and rhodamine 6G, respectively. Laser peak intensity as a function of pump power (empty blue circles) and evolution of emission linewidth with pump power (full green circles). The yellow and red rectangle illustrate the lasing region above threshold ($P = 38$ mJ cm^{-2} for fluorescein and for $P = 7$ mJ cm^{-2} for rhodamine). b,d) Comparison of spectra above threshold and in fluorescence.

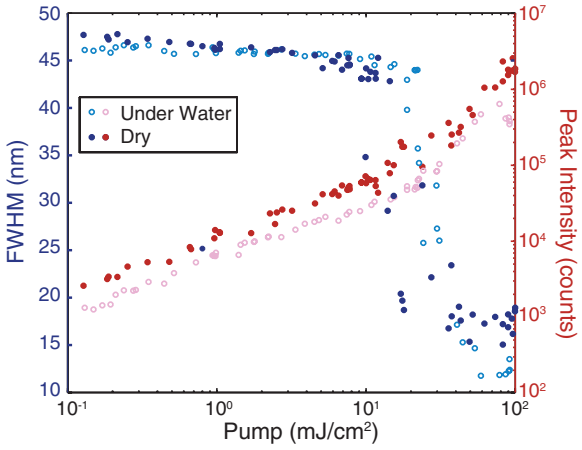

Figure 4. Lasing action for rhodamine-doped silk random laser in air (dark blue and red full circles) and water (light blue and pink open circles). The blue open and full circles are the FWHM plotted versus pump power, while the full red and open pink circles are the peak intensity. When the device is immersed in water the lasing threshold is shifted toward larger values (≈50% increase) consistent with the theoretical prediction (≈30% increase), as detailed in the Supporting Information.

reduced as compared to air-operation because of the decrease index of refraction contrast. An increase by a factor of 3–4 in l_t is predicted theoretically (Figure S2a, Supporting Information) leading to an increase of threshold by 30% (Figure S2b, Supporting Information). Nevertheless, random lasing action can still be achieved experimentally, albeit with a slightly larger threshold (≈50% increase) as shown in **Figure 4**. In fact the smaller light confinement is partially compensated by a larger diffusive volume explored by the emitted light, therefore lasing operation is still achieved with low thresholds.

A biocompatible silk random laser is an ideal candidate for future generation biological sensing. Random lasing sensing applications have been explored already, but limited as they rely on detectable change in scattering strength which modifies the lasing properties, as shown for cancerous tissue,[11] and polymer dispersed liquid crystals.[28] Instead, a more flexible and powerful sensing scheme would rely on a change in the gain molecule itself. We propose here a silk-based biolaser as a standalone device compatible with integration in living tissue.

In **Figure 5** we show a proof-of-principle laser capable of sensing pH, across a broad range of NaOH concentrations, in an aqueous environment. At increasing pH the lasing properties of rhodamine are degraded, showing a nonlinear transition of the spectral properties at around pH ≈11, from 15–20 nm full width at half maximum (FWHM) at pH 7 to ≈55 nm FWHM at pH ≈13. We attribute this effect to a change in the gain medium, as induced by deprotonation of the dye molecule, and not to a structural or refractive index modification. Total transmission experiments at high pH indicate only a 7% decrease of the scattering strength as compared to pH 7, which alone would induce a threshold change of only a few percent. Scanning electron microscopy images confirm that the porous structure shown in Figure 1c is not visibly altered by the increasing pH. Moreover, the lasing switching off by increasing pH is reversible: when the sample is irrigated with deionized water for 1 h, the lasing action is recovered.

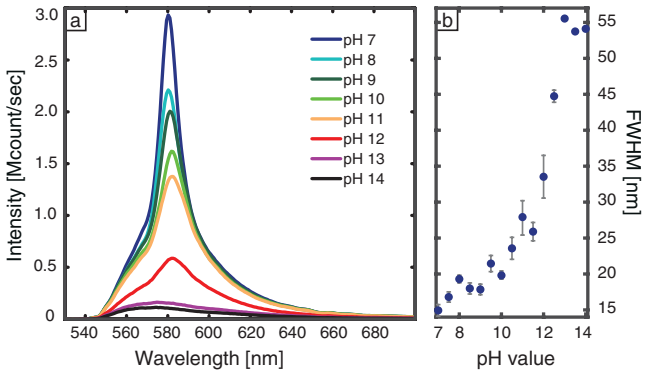

Figure 5. a) Lasing spectra from rhodamine-doped silk random laser in aqueous solution, for a fixed pump power of 60 mJ cm^{-2}, and various molarities of NaOH dissolved in the solution which changes the solution pH. b) Evolution of the FWHM of the emission versus pH. The error bars are the standard deviation of the average of ten measurements per point.

The silk-based inverted photonic glass geometry as described here is promising for sensing applications as it is a porous random laser, largely insensitive to external shape, potentially as small as the ≈10 × 10 μm^2 (10 μm is the calculated critical length, $(L_{cr} = \pi\sqrt{\ell_g \ell_t/3})$, see the Experimental Section) and more importantly very flexible to host different dyes with sensing capabilities encapsulated in the silk matrix. In vivo application will require sensitivity in the physiological pH range 7–9 and further cytotoxicity tests, what provided here is a proof-of-principle demonstration which illustrates a possible path for further refinement.

In conclusion, we have presented a novel biocompatible random lasing device made entirely of doped silk, obtained by solely using self-assembly techniques, with potential for sensitive sensing. Surprisingly, the complexity of the disordered medium leads to a great simplicity of the overall device. Moreover, the random lasing device is compatible with aqueous environments and living tissues due to its disordered structure and its biocompatible constituents. We believe that random lasing devices made of silk could eventually be integrated in biological tissues or on-skin for bioengineering applications with the potential to provide a new tool to image and sense biological properties inside human body. A silk random lasing biosensor is made from all-natural materials and is processed with water and toluene at room temperature. Therefore, it is an environmentally friendly product, cheap, and easily mass-produced, that has the potential to be at the basis of future silk-biophotonic applications in technology and medicine.

Experimental Section

Silk Fibroin Solution Preparation: Silk fibroin solution was prepared as previously described.[14] In brief, *B. Mori* silkworm cocoons were boiled for 30 min in a solution of 0.02 M Na_2CO_3 to remove sericin. The extracted fibroin fibers were rinsed in deionized water, set to dry for 24 h, and then dissolved in a 9.3 M LiBr aqueous solution at 60 °C for 3 h. The solution was dialyzed against deionized water using dialysis cassettes (Slide-a-Lyzer, Pierce, MWCO 3.5 kDa) at room temperature for 2 d. The obtained fibroin solution (≈70 mg mL^{-1}) was purified using

centrifugation and filtered through a 5 μm syringe filter to remove processing debris.

Inverse Photonic Glass Fabrication: The dyes, rhodamine 6G and sodium fluorescein were dissolved in deionized water and sequentially added to a solution of silk in water (3–7%wt), such that the dry ratio is 99.5%wt of silk and 0.5%wt of dye. Therefore, the final amount of dye in the samples discussed is <0.3 mg, which corresponds to ≈10 ng for a $100 \times 100 \times 100$ μm^3 sample; less than 0.1 mg mL^{-1} is considered a nontoxic amount of fluorescein. The growth method employed is similar to that reported for photonic glass.[5] Here, a mixed direct photonic glass of polystyrene spheres and silk was first grown, and then the inverse photonic glass structure was obtained by removing the sphere via selective chemical etching in toluene. A colloidal solution of aqueous doped silk and polystyrene spheres (1.28 μm diameter) of 10%wt, was casted inside a cylindrical mold of 1 cm diameter, made of Teflon and left to dry in the oven at 45 °C for 24 h. The spheres arrange in a solid packing, with a final filling fraction of ≈45%–55% estimated by volume measurements via electron microscopy. Once dry, the sample was chemically etched in a 99% toluene solution for 72 h, which dissolves the polystyrene spheres while leaving the silk unaffected, a small fraction of the dye was released to the toluene solution during the etching, while dye leaching was much reduced after this process. In addition, the silk nanostructured material can be made free-standing with no loss of functionalities, by simply growing the material over a polystyrene film cast on the glass substrate, film which was then dissolved during the same sphere etching process. Silk was crystallized by exposing it to water vapor for 12 h in a vacuum desiccator.[29]

Scattering Measurement: The scattering properties of the material were assessed by total transmission measurements via an integrating sphere fiber coupled to a spectrometer which records the light transmitted by the sample at all directions, as a function of light frequency, as previously described in ref. [20]. The total transmission at each wavelength follows the photonic Ohm's law, that is

$$T(L,\lambda) = \frac{1}{\alpha z_e} \frac{\sinh\left[\alpha\left(z_p + z_e\right)\right]\sinh(\alpha z_e)}{\sinh\left[\alpha\left(L + 2z_e\right)\right]} \tag{1}$$

where α is the reciprocal of the absorption length, L is the sample thickness, z_p is the penetration length (here taken to be equal to z_e), and z_e is the extrapolation length, which is given by where R is the averaged reflectivity (R = 0.39 assuming a filling fraction of ≈50%).[30] A fit to Equation (1), for different sample thickness, gives the transport mean free path in the sample and the absorption length.

Scattering Calculations: Calculations of the transport mean free path in the inverted photonic glass were obtained by Mie solution of the Maxwell equations.[31] First, the frequency-dependent scattering cross section σ was calculated and then the transport mean free path was obtained by considering the angular scattering pattern via

$$z_e = \frac{1}{2\alpha}\ln\left(\frac{1+\alpha z_0}{1-\alpha z_0}\right),\ z_0 = \frac{2}{3}\ \ell_t \frac{1+R}{1-R} \tag{2}$$

$$\ell_t = \frac{1}{\rho\sigma\left(1-\langle\cos\theta\rangle\right)} \tag{3}$$

where ρ is the scatterers density, and θ the scattering angle. The theoretical model is limited by the independent scattering approximation as it describes the scatterers as if they were embedded in a homogenous medium. Furthermore, it neglects any recurrent scattering events, which is justified as $kl_t \approx 40$–60 is much larger than unity. The spheres size polydispersity is taken into account by means of a convolution with a gaussian distribution with a 2% standard deviation. The time photons are trapped inside the sample, which is the Thouless time given by $\tau = (1/8)(L^2/D)$ (for a slab of thickness L and diffusion constant D), and is of the order of 10 ps while the excitation pulses are 6 ns long. The critical length required to fulfill the condition of gain larger than losses can be calculated to be $(L_{cr} = \pi\sqrt{\ell_g \ell_t / 3})$ which is ≈10 μm, therefore a medium as small as $\approx 10 \times 10$ μm^2 would be enough to achieve lasing.

Random Lasing Measurement: The samples were pumped with single pulses of the second harmonic of an Nd:YAG Q-switched pulsed laser, at 532 nm wavelength, 10 Hz repetition rate, and 6 ns pulse duration. The pump diameter is ≈2 mm. The detection software registers pulse power and sample emission spectra in backscattering for each pulse. The large energy range of 5–6 orders of magnitude is achieved by a combination of neutral density filters for the coarse control and a half-waveplate and a polarizer for the fine control. From the spectral evolution of the emission one can extract the relevant lasing parameters such as the lasing threshold. The threshold of the random lasing is defined as the power for which the spectral width reduces to half than its low-pump power value. Threshold is often identified with the intercept of a linear fit to the above-threshold part of the peak power versus pump power. The definition overestimates the thresholds but is simpler and more robust against measurement noise. The compound proves to be stable over many excitation cycles and no significant difference is observed in the results besides a small dye bleaching (1/e decay after ≈2400 or ≈13 600 lasing cycles for fluorescein and rhodamine, respectively). In addition, the device is capable of lasing even after being stored for one year.

Supporting Information

Supporting Information is available from the Wiley Online Library or from the author.

Acknowledgements

S.C., M.G., and B.M. contributed equally to this work. The authors wish to thank Greg Wurtz and Giuseppe Marino for fruitful discussions. This research was funded by the Engineering and Physical Sciences Research Council (EPSRC), the Leverhulme Trust, Royal Society, and the FP7 EU Project People. F.G.O. would like to acknowledge the Office of Naval Research for support of this work (N00014-13-1-0596). Open access for this article was funded by King's College London.

Received: March 16, 2016
Published online: April 21, 2016

[1] R. Sapienza, P. D. Garcia, J. Bertolotti, M. D. Martin, A. Blanco, L. Vina, C. Lopez, D. S. Wiersma, *Phys. Rev. Lett.* **2007**, *99*, 233902.
[2] S. Nizamoglu, M. C. Gather, S. H. Yun, *Adv. Mater.* **2013**, *25*, 5943.
[3] C. Vannahme, F. Maier-Flaig, U. Lemmer, A. Kristensen, *Lab Chip* **2013**, *13*, 2675.
[4] M. Schubert, A. Steude, P. Liehm, N. M. Kronenberg, M. Karl, E. C. Campbell, S. J. Powis, M. C. Gather, *Nano Lett.* **2015**, *15*, 5647.
[5] M. Humar, S. H. Yun, *Nat. Photonics* **2015**, *9*, 572.
[6] D. S. Wiersma, *Nat. Phys.* **2008**, *4*, 359.
[7] H. Cao, *J. Phys. A* **2005**, *38*, 10497.
[8] I. Viola, N. Ghofraniha, A. Zacheo, V. Arima, C. Conti, G. Gigli, *J. Mater. Chem. C* **2013**, *1*, 8128.
[9] R. Zhang, S. Knitter, S. F. Liew, F. G. Omenetto, B. M. Reinhard, H. Cao, L. Dal Negro, *Appl. Phys. Lett.* **2016**, *108*, 011103.
[10] Q. Song, S. Xiao, Z. Xu, J. Liu, X. Sun, V. Drachev, V. M. Shalaev, O. Akkus, Y. L. Kim, *Opt. Lett.* **2010**, *35*, 1425.
[11] R. C. Polson, Z. V. Vardeny, *Appl. Phys. Lett.* **2004**, *85*, 1289.
[12] F. G. Omenetto, D. L. Kaplan, *Nat. Photonics* **2008**, *2*, 641.
[13] F. G. Omenetto, D. L. Kaplan, *Science* **2010**, *329*, 528.
[14] D. N. Rockwood, R. C. Preda, T. Yücel, X. Wang, M. L. Lovett, D. L. Kaplan, *Nat. Protoc.* **2011**, *6*, 1612.
[15] H. Tao, D. L. Kaplan, F. G. Omenetto, *Adv. Mater.* **2012**, *24*, 2824.
[16] S. Kim, A. N. Mitropoulos, J. D. Spitzberg, H. Tao, D. L. Kaplan, F. G. Omenetto, *Nat. Photonics* **2012**, *6*, 818.

[17] J. P. Mondia, J. J. Amsden, D. Lin, L. Dal Negro, D. L. Kaplan, F. G. Omenetto, *Adv. Mater.* **2010**, *22*, 4596.
[18] S. Toffanin, S. Kim, S. Cavallini, M. Natali, V. Benfenati, J. J. Amsden, D. L. Kaplan, R. Zamboni, M. Muccini, F. G. Omenetto. *Appl. Phys. Lett.* **2012**, *101*, 091110.
[19] R. R. da Silva, C. T. Dominguez, M. V. dos Santos, R. Barbosa-Silva, M. Cavicchioli, L. M. Christovan, L. S. A. de Melo, A. S. L. Gomes, C. B. de Araujo, S. J. L. Ribeiro, *J. Mater. Chem. C* **2013**, *1*, 7181.
[20] P. D. Garcia, R. Sapienza, Á. Blanco, C. López, *Adv. Mater.* **2007**, *19*, 2597.
[21] J. F. Galisteo-López, M. Ibisate, R. Sapienza, L. S. Froufe-Perez, *Adv. Mater.* **2011**, *23*, 30.
[22] P. J. Saine, M. E. Tyler, *Ophthalmic Photography: Retinal Photography, Angiography, and Electronic Imaging*, 2nd ed., Butterworth-Heinemann, Boston, MA, USA **2002**, Ch. 4.
[23] M. Leonetti, R. Sapienza, M. Ibisate, C. Conti, C. Lopez, *Opt. Lett.* **2009**, *34*, 3764.
[24] A. Tulek, R. C. Polson, Z. V. Vardeny, *Nat. Phys.* **2010**, *6*, 303.
[25] R. G. S. El-Dardiry, A. Lagendijk, *Appl. Phys. Lett.* **2011**, *98*, 161106.
[26] S. Gottardo, R. Sapienza, P. D. Garcia, A. Blanco, D. S. Wiersma, C. Lopez, *Nat. Photonics* **2008**, *7*, 102.
[27] M. Gaio, M. Peruzzo, R. Sapienza, *Opt. Lett.* **2015**, *40*, 1611.
[28] D. S. Wiersma, S. Cavalieri, *Nature* **2001**, *414*, 708.
[29] X. Hu, K. Shmelev, L. Sun, E. S. Gil, S. H. Park, P. Cebe, D. L. Kaplan, *Biomacromolecules* **2011***12*, 1686.
[30] X. Zhu, D. J. Pine, D. A. Weitz, *Phys. Rev. A* **1991**, *44*, 3948.
[31] C. F. Bohren, D. R. H. Bohren, *Absorption and Scattering of Light by Small Particles*, Wiley-VCH, New York **1983**, Ch. 4.